JOC Article

Nucleophilicity and Leaving-Group Ability in Frontside and Backside S_N2 Reactions

A. Patrícia Bento and F. Matthias Bickelhaupt*

Department of Theoretical Chemistry and Amsterdam Center for Multiscale Modeling, Scheikundig Laboratorium der Vrije Universiteit, De Boelelaan 1083, NL-1081 HV Amsterdam, The Netherlands

fm.bickelhaupt@few.vu.nl

Received June 7, 2008

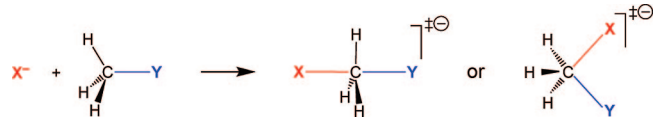

Nucleophilic substitution is ubiquitous in chemistry and well studied. Nucleophilicity and leaving-group ability have been related to various reactant properties, such as electronegativity, size, polarizability, and others. Yet, the state-of-the-art is to some extent still phenomenological. Here, we try to arrive at a straightforward, causal relationship between the reactants' electronic structure and their S_N2 reactivity. To this end, we have explored the potential energy surfaces of the backside as well as frontside S_N2 reactions of $X^- + CH_3Y$ with X, Y = F, Cl, Br, and I, using relativistic density functional theory (DFT) at ZORA-OLYP/TZ2P. These explorations provide us with a consistent overview of trends, over a wide range of reactivities and pathways, which were analyzed using the activation strain model of chemical reactivity. A clear picture emerges from these analyses: nucleophilicity is determined by the electron-donor capability of the nucleophile (i.e., energy and shape of the X^- np atomic orbital), and leaving-group ability derives directly from carbon–leaving group (C−Y) bond strength.

1. Introduction

Bimolecular nucleophilic substitution (S_N2, Scheme 1) reactions are featured in many routes in organic synthesis.[1] Over the past decades, various experimental and theoretical studies have been conducted to explore trends in reactivity as well as the nature of the S_N2 potential energy surface (PES).[2−8] In the late 1970s, Olmstead and Brauman[7] proposed the double-well PES for gas-phase S_N2 reactions, which is characterized by reactant and product complexes (RC, PC) that are separated by a central transition state (TS). This is shown in Scheme 2 for a thermoneutral (X = Y) as well as an exothermic (X ≠ Y) S_N2 reaction. The barrier in the latter may disappear if the process becomes sufficiently exothermic, as shown in Scheme 2c.

Many factors play a role in determining the efficiency of an S_N2 reaction, for example, the steric demand and/or effective electronegativity of the substituents at the central carbon atom (or in the nucleophile and leaving group) or the central atom itself which may be, for example, N, Si, P, or S instead of C. The regular backside S_N2-b substitution, which goes with inversion of configuration at carbon (cf. Walden inversion), is in general significantly more efficient; that is, it has a lower reaction barrier than the corresponding frontside S_N2-f pathway, which goes with retention of configuration. The nature of condensed-phase S_N2 mechanisms furthermore strongly depends on solvation effects.

In the present study, we focus on yet two other factors, namely, nucleophilicity and leaving-group ability. These properties refer to how good a nucleophile or leaving group is in the sense of yielding a low barrier to S_N2 substitution. Nucleophilicity and leaving-group ability have been related to various properties of X^- and Y^- (Scheme 1), such as electronegativity, size, polarizability, and others. Yet, the state-of-the-art is to some extent still phenomenological.[1,9] Here, we try to arrive at a straightforward, causal relationship between the reactants' electronic structure and their S_N2 reactivity. To this end, we have explored the potential energy surfaces of the backside (S_N2-b) as well as frontside (S_N2-f) nucleophilic substitution reactions of $X^- + CH_3Y$ with X and Y = F, Cl, Br, and I, using relativistic density functional theory (DFT) at ZORA-OLYP/TZ2P as implemented in the Amsterdam Density Functional

* To whom correspondence should be addressed. Fax: +31-20-59 87629.

(1) (a) Smith, M. B.; March, J. *March's Advanced Organic Chemistry: Reactions, Mechanisms, and Structure*; Wiley: New York, 2007. (b) Carey, F. A.; Sundberg, R. J. *Advanced Organic Chemistry, Part A*; Springer: New York, 2007. (c) Lowry, T. H.; Richardson, K. S. *Mechanism and Theory in Organic Chemistry*; Harper and Row: New York, 1987. (d) Ingold, C. *Structure and Mechanism in Organic Chemistry*; Cornell University Press: Ithaca, NY, 1969.

(2) Angel, L. A.; Ervin, K. M. *J. Phys. Chem. A* **2001**, *105*, 4042.

10.1021/jo801215z CCC: $40.75
Published on Web 08/09/2008

SCHEME 1. Model Reaction Systems

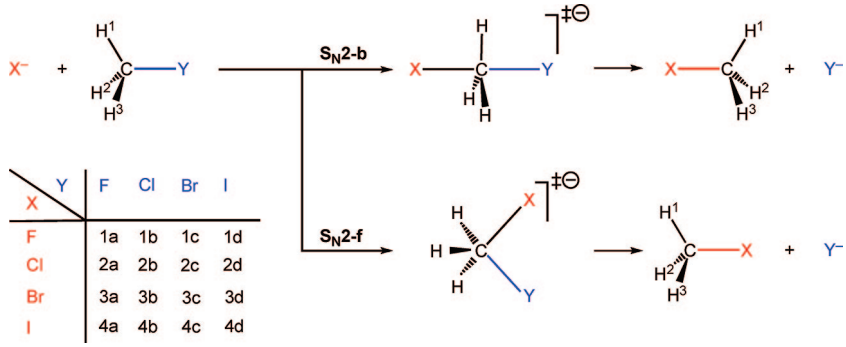

X \ Y	F	Cl	Br	I
F	1a	1b	1c	1d
Cl	2a	2b	2c	2d
Br	3a	3b	3c	3d
I	4a	4b	4c	4d

(ADF) program. Scheme 1 provides an overview of all model systems and our nomenclature.

The explorations of our S_N2-b and S_N2-f model reactions provide us with an overview of trends in reaction energies and barriers, over a wide range of reactivities and pathways, all obtained consistently with one and the same method. This nicely augments the existing experimental and theoretical data and constitutes an objective on its own. However, the main purpose, as pointed out above, is to obtain a qualitative, physical understanding of the trends in reactivity and, in particular, the concepts of nucleophilicity and leaving-group ability. This is achieved through an analysis of the PESs using the activation strain model of chemical reactivity in which the potential energy surface $\Delta E(\zeta)$ is decomposed, along the reaction coordinate ζ, into the strain $\Delta E_{strain}(\zeta)$ associated with deforming the individual reactants plus the actual interaction $\Delta E_{int}(\zeta)$ between the deformed reactants: $\Delta E(\zeta) = \Delta E_{strain}(\zeta) + \Delta E_{int}(\zeta)$ (see Theoretical Methods for details).

A clear picture emerges from these analyses. They show that nucleophilicity is determined in a straightforward manner by the electron-donor capability of the nucleophile (i.e., energy and shape of the X^- np atomic orbital), while leaving-group ability derives directly from the carbon–leaving group (C−Y) bond strength.

2. Theoretical Methods

2.1. Computational Details. All calculations were performed with the Amsterdam Density Functional (ADF) program developed by Baerends and others.[10,11] The molecular orbitals (MOs) were expanded in a large uncontracted set of Slater-type orbitals (STOs) containing diffuse functions, TZ2P. This basis is of triple-ζ quality and has been augmented by two sets of polarization functions: 2p and 3d on hydrogen, 3d and 4f on carbon, fluorine, and chlorine, 4d and 4f on bromine, and 5d and 4f on iodine. The core shells of carbon (1s), fluorine (1s), chlorine (1s2s2p), bromine (1s2s2p3s3p), and iodine (1s2s2p3s3p3d4s4p) were treated by the frozen-core approximation.[11] An auxiliary set of s, p, d, f, and g STOs was used to fit the molecular density and to represent the Coulomb and exchange potentials accurately in each SCF cycle. Relativistic effects were accounted by using the zeroth-order approximation (ZORA).[12]

Equilibrium and transition-state geometries were fully optimized at the OLYP[13] density functional, which involves Handy's optimized exchange, OPTX. This level of theory was previously shown to agree satisfactorily with highly correlated ab initio benchmarks.[14] All stationary points were confirmed by vibrational analysis:[15] for equilibrium structures, all normal modes have real frequencies, whereas transition states[16] have one normal mode with an imaginary frequency. Furthermore, transition states were verified to connect

(3) (a) Angel, L. A.; Ervin, K. M. *J. Phys. Chem. A* **2004**, *108*, 9827. (b) Bach, R. D.; Dmitrenko, O.; Thorpe, C. *J. Org. Chem.* **2008**, *73*, 12. (c) Botschwina, P. *Theor. Chem. Acc.* **1998**, *99*, 426. (d) Carvalho, A. T. P.; Swart, M.; van Stralen, J. N. P.; Fernandes, P. A.; Ramos, M. J.; Bickelhaupt, F. M. *J. Phys. Chem. B* **2008**, *112*, 2511. (e) Chabinyc, M. L.; Craig, S. L.; Regan, C. K.; Brauman, J. I. *Science* **1998**, *279*, 1882. (f) Chandrasekhar, J.; Smith, S. F.; Jorgensen, W. L. *J. Am. Chem. Soc.* **1985**, *107*, 154. (g) DePuy, C. H.; Gronert, S.; Mulin, A.; Bierbaum, V. M. *J. Am. Chem. Soc.* **1990**, *112*, 8650. (h) Glukhovtsev, M. N.; Pross, A.; Radom, L. *J. Am. Chem. Soc.* **1995**, *117*, 2024. (i) Glukhovtsev, M. N.; Pross, A.; Radom, L. *J. Am. Chem. Soc.* **1996**, *118*, 6273. (j) Glukhovtsev, M. N.; Pross, A.; Schlegel, H. B.; Bach, R. D.; Radom, L. *J. Am. Chem. Soc.* **1996**, *118*, 11258. (k) Gonzales, J. M.; Pak, C.; Cox, R. S.; Allen, W. D.; Schaefer, H. F., III; Császár, A. G.; Tarczay, G. *Chem.—Eur. J.* **2003**, *9*, 2173. (l) Gronert, S. *Acc. Chem. Res.* **2003**, *36*, 848. (m) Harder, S.; Streitwieser, A.; Petty, J. T.; Schleyer, P. v. R. *J. Am. Chem. Soc.* **1995**, *117*, 3253. (n) Laerdahl, J. K.; Uggerud, E. *Int. J. Mass Spectrom.* **2002**, *214*, 277. (o) Lee, I.; Kim, C. K.; Sohn, C. K.; Li, H. G.; Lee, H. W. *J. Phys. Chem. A* **2002**, *106*, 1081. (p) Li, C.; Ross, P.; Szulejko, J. E.; McMahon, T. B. *J. Am. Chem. Soc.* **1996**, *118*, 9360. (q) Nibbering, N. M. M. *Acc. Chem. Res.* **1990**, *23*, 279. (r) Norton, S. H.; Bachrach, S. M.; Hayes, J. M. *J. Org. Chem.* **2005**, *70*, 5896. (s) Ren, Y.; Yamataka, H. *Chem. Eur. J.* **2007**, *13*, 677. (t) Schmatz, S. *ChemPhysChem* **2004**, *5*, 600. (u) Schmatz, S.; Botschwina, P.; Stoll, H. *Int. J. Mass Spectrom.* **2000**, *201*, 277. (v) Shaik, S. S.; Schlegel, H. B.; Wolfe, S. *Theoretical Aspects of Physical Organic Chemistry: The S_N2 Mechanism*; Wiley: New York, 1992. (w) Su, T.; Wang, H.; Hase, W. L. *J. Phys. Chem. A* **1998**, *102*, 9819. (x) van Bochove, M. A.; Bickelhaupt, F. M. *Eur. J. Org. Chem.* **2008**, 649. (y) van Bochove, M. A.; Swart, M.; Bickelhaupt, F. M. *J. Am. Chem. Soc.* **2006**, *128*, 10738. (z) van Bochove, M. A.; Swart, M.; Bickelhaupt, F. M. *ChemPhysChem* **2007**, *8*, 2452. (aa) Vayner, G.; Houk, K. N.; Jorgensen, W. L.; Brauman, J. I. *J. Am. Chem. Soc.* **2004**, *126*, 9054. (bb) Wang, H.; Hase, W. L. *J. Am. Chem. Soc.* **1997**, *119*, 3093. (cc) Wladkowski, B. D.; Allen, W. D.; Brauman, J. I. *J. Phys. Chem.* **1994**, *98*, 13532. (dd) Uggerud, E. *Chem.—Eur. J.* **2006**, *12*, 1127.

(4) Bento, A. P.; Bickelhaupt, F. M. *J. Org. Chem.* **2007**, *72*, 2201.

(5) Bickelhaupt, F. M. *J. Comput. Chem.* **1999**, *20*, 114.

(6) (a) Deng, L.; Branchadell, V.; Ziegler, T. *J. Am. Chem. Soc.* **1994**, *116*, 10645. (b) Bickelhaupt, F. M.; Hermann, H.; Boche, G. *Angew. Chem.* **2006**, *118*, 838; *Angew. Chem., Int. Ed.* **2006**, *45*, 823.

(7) Olmstead, W. N.; Brauman, J. I. *J. Am. Chem. Soc.* **1977**, *99*, 4219.

(8) Bento, A. P.; Bickelhaupt, F. M. *Chem. Asian J.* **2008**, *3*, in press.

(9) According to the IUPAC Gold Book, nucleophilicity is the relative reactivity of nucleophilic reagent and the leaving-group ability (nucleofugality) is the tendency of atoms or groups to depart with the bonding electron pair.

(10) *Computer code ADF 2007.01*; Baerends, E. J. SCM: Amsterdam, The Netherlands; Fonseca Guerra, C.; Snijders, J. G.; te Velde, G.; Baerends, E. J. *Theor. Chem. Acc.* 1998, *99*, 391.

(11) (a) Baerends, E. J.; Ellis, D. E.; Ros, P. *Chem. Phys.* **1973**, *2*, 41. (b) te Velde, G.; Bickelhaupt, F. M.; Baerends, E. J.; Fonseca Guerra, C.; van Gisbergen, S. J. A.; Snijders, J. G.; Ziegler, T. *J. Comput. Chem.* **2001**, *22*, 931.

(12) van Lenthe, E.; Baerends, E. J.; Snijders, J. G. *J. Chem. Phys.* **1994**, *101*, 9783.

(13) (a) Handy, N. C.; Cohen, A. J. *Mol. Phys.* **2001**, *99*, 403. (b) Lee, C.; Yang, W.; Parr, R. G. *Phys. Rev. B* **1988**, *37*, 785.

(14) (a) Baker, J.; Pulay, P. *J. Chem. Phys.* **2002**, *117*, 1441. (b) Bento, A. P.; Solà, M.; Bickelhaupt, F. M. *J. Comput. Chem.* **2005**, *26*, 1497. (c) Gonzales, J. M.; Allen, W. D.; Schaefer, H. F., III *J. Phys. Chem. A* **2005**, *109*, 10613. (d) Grüning, M.; Gritsenko, O. V.; Baerends, E. J. *J. Phys. Chem. A* **2004**, *108*, 4459. (e) Swart, M.; Ehlers, A. W.; Lammertsma, K. *Mol. Phys.* **2004**, *102*, 2467. (f) Xu, X.; Goddard, W. A., III *J. Phys. Chem. A* **2004**, *108*, 8495.

(15) Fan, L.; Versluis, L.; Ziegler, T.; Baerends, E. J.; Ravenek, W. *Int. J. Quantum Chem. Quantum Chem. Symp.* **1988**, *S22*, 173.

(16) Fan, L.; Ziegler, T. *J. Chem. Phys.* **1990**, *92*, 3645.

SCHEME 2. S_N2 Potential Energy Surfaces: (a) Thermoneutral, (b) Exothermic with Central Barrier, (c) Exothermic without Central Barrier[a]

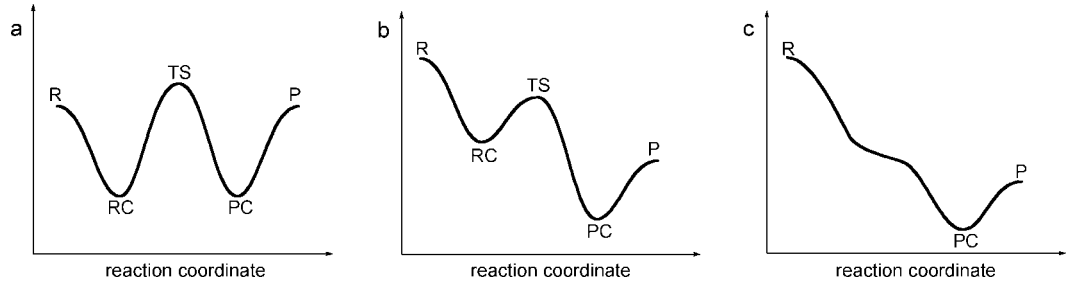

[a] R, RC, TS, PC, and P stand for reactants, reactant complex, transition state, product complex, and products, respectively.

TABLE 1. Energies (in kcal mol^{-1}) Relative to Reactants of the Stationary Points Occurring in Backside and Frontside S_N2 Reactions of $X^- + CH_3Y$[a]

X	species	Y =	F a	Cl b	Br c	I d
F	RC-b		−15.7	−19.4	[b]	[b]
1	**TS-b**		**−7.6**	**−19.2**	[b]	[b]
	PC-b		−15.7	−43.6	−51.9	−57.8
	P		0.0	−36.0	−45.8	−52.5
	TS-H		−15.5	−19.0	−21.0	−22.7
	RC-f		−17.5	−21.3	−22.8	−24.5
	TS-f		**33.4**	**19.4**	**12.7**	**7.9**
	PC-f		−17.5	[b]	[b]	[b]
Cl	RC-b		−7.6	−9.0	−10.0	−10.8
2	**TS-b**		**16.8**	**−0.2**	**−5.6**	**−8.6**
	PC-b		16.7	−9.0	−17.0	−22.6
	P		36.0	0.0	−9.7	−16.5
	TS-H		17.1	[b]	[b]	[b]
	RC-f		[b]	[b]	[b]	[b]
	TS-f		**55.4**	**40.2**	**33.5**	**28.9**
	PC-f		14.8	[b]	[b]	[b]
Br	RC-b		−6.2	−7.3	−8.0	−8.6
3	**TS-b**		[b]	**4.1**	**−1.7**	**−5.0**
	PC-b		[b]	−0.2	−8.0	−13.4
	P		45.8	9.7	0.0	−6.7
	TS-H		24.8	[b]	[b]	[b]
	RC-f		[b]	[b]	[b]	[b]
	TS-f		**58.4**	**43.3**	**36.6**	**32.0**
	PC-f		22.9	[b]	[b]	[b]
I	RC-b		−5.2	−6.2	−6.7	−7.3
4	**TS-b**		[b]	**7.9**	**1.8**	**−1.9**
	PC-b		[b]	5.7	−1.9	−7.3
	P		52.5	16.5	6.7	0.0
	TS-H		29.8	[b]	[b]	[b]
	RC-f		[b]	[b]	[b]	[b]
	TS-f		**60.4**	**45.4**	**38.8**	**34.2**
	PC-f		28.0	[b]	[b]	[b]

[a] Computed at ZORA-OLYP/TZ2P. See Scheme 1 for numbering of species. [b] Nonexistent.

the supposed educt and product minima by carrying out intrinsic reaction coordinate (IRC) calculations.[17]

2.2. Analysis of the Potential Energy Surfaces. Insight into how the activation barriers arise is obtained through activation strain analyses of the various S_N2 reactions.[5,18] The activation strain model[5,18] is a fragment approach to understanding chemical reactions, in which the height of reaction barriers is described and understood in terms of the original reactants. Thus, the potential energy surface $\Delta E(\zeta)$ is decomposed, along the reaction coordinate ζ, into the strain $\Delta E_{strain}(\zeta)$ associated with deforming the individual reactants plus the actual interaction $\Delta E_{int}(\zeta)$ between the deformed reactants:

$$\Delta E(\zeta) = \Delta E_{strain}(\zeta) + \Delta E_{int}(\zeta)$$

The strain $\Delta E_{strain}(\zeta)$ is determined by the rigidity of the reactants and on the extent to which groups must reorganize in a particular reaction mechanism, whereas the interaction $\Delta E_{int}(\zeta)$ between the reactants depends on their electronic structure and on how they are mutually oriented as they approach each other. It is the interplay between $\Delta E_{strain}(\zeta)$ and$\Delta E_{int}(\zeta)$ that determines if and at which point along the ζ a barrier arises. The activation energy of a reaction $\Delta E^{\ddagger} = \Delta E(\zeta^{TS})$ consists of the activation strain $\Delta E^{\ddagger}_{strain} = \Delta E_{strain}(\zeta^{TS})$ plus the TS interaction $\Delta E^{\ddagger}_{int} = \Delta E_{int}(\zeta^{TS})$:

$$\Delta E^{\ddagger} = \Delta E^{\ddagger}_{strain} + \Delta E^{\ddagger}_{int}$$

In the graphical representations shown below, ζ is then projected onto the stretch of the carbon–leaving group (C−Y) bond, which is generally one of the dominant components of the reaction coordinate and undergoes a well-defined change from an intact to a dissociated bond.

The interaction $\Delta E_{int}(\zeta)$ between the strained reactants is further analyzed in the conceptual framework provided by the Kohn−Sham molecular orbital (KS-MO) model.[19−21] To this end, it is further decomposed into three physically meaningful terms:

$$\Delta E_{int}(\zeta) = \Delta V_{elstat} + \Delta E_{Pauli} + \Delta E_{oi}$$

The term ΔV_{elstat} corresponds to the classical electrostatic interaction between the unperturbed charge distributions of the deformed reactants and is usually attractive. The Pauli repulsion ΔE_{Pauli} comprises the destabilizing interactions between occupied orbitals and is responsible for any steric repulsion (see ref 20 for an exhaustive discussion). The orbital interaction ΔE_{oi} accounts for charge transfer (interaction between occupied orbitals on one moiety with unoccupied orbitals on the other, including HOMO−LUMO interactions) and polarization (empty-occupied orbital mixing on one fragment due to the presence of another fragment). Since the Kohn−Sham MO method of density functional theory (DFT) in principle yields exact energies and, in practice, with the available density functionals for exchange and correlation, rather accurate, we have the special situation that a seemingly one-particle model (an MO method) in principle fully accounts for the bonding energy.[19,20]

(17) Fukui, K. *Acc. Chem. Res.* **1981**, *14*, 363.
(18) (a) de Jong, G. Th.; Bickelhaupt, F. M. *ChemPhysChem* **2007**, *8*, 1170. (b) Diefenbach, A.; Bickelhaupt, F. M. *J. Chem. Phys.* **2001**, *115*, 4030. (c) Diefenbach, A.; de Jong, G. Th.; Bickelhaupt, F. M. *J. Chem. Theory Comput.* **2005**, *1*, 286.
(19) Baerends, E. J.; Gritsenko, O. V. *J. Phys. Chem. A* **1997**, *101*, 5383.
(20) Bickelhaupt, F. M.; Baerends E. J. In *Reviews in Computational Chemistry*; Lipkowitz, K. B., Boyd, D. B., Eds.; Wiley-VCH: New York, 2000; Vol. 15, pp 1−86.
(21) (a) Bickelhaupt, F. M.; Nibbering, N. M. M.; van Wezenbeek, E. M.; Baerends, E. J. *J. Phys. Chem.* **1992**, *96*, 4864. (b) Bickelhaupt, F. M.; Diefenbach, A.; de Visser, S. P.; de Koning, L. J.; Nibbering, N. M. M. *J. Phys. Chem. A* **1998**, *102*, 9549. (c) Ziegler, T.; Rauk, A. *Theor. Chim. Acta* **1977**, *46*, 1. (d) Ziegler, T.; Rauk, A. *Inorg. Chem.* **1979**, *18*, 1558. (e) Ziegler, T.; Rauk, A. *Inorg. Chem.* **1979**, *18*, 1755.

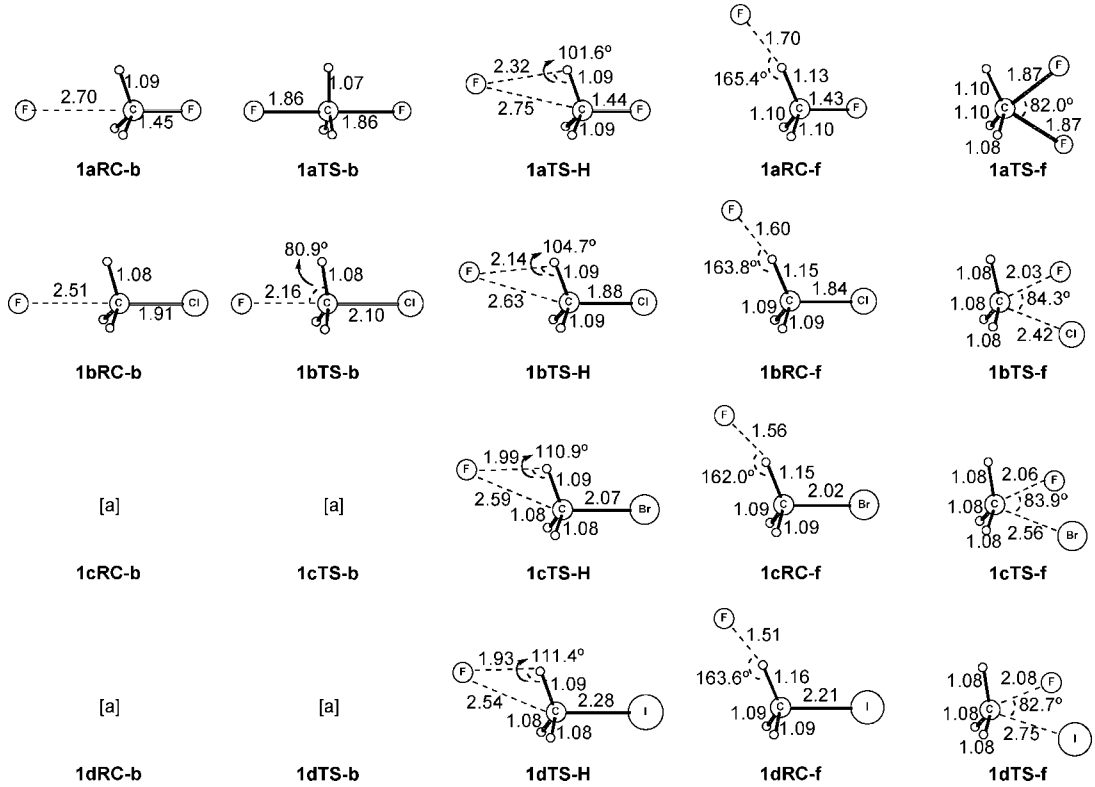

FIGURE 1. Structures (in angstroms, degrees) of stationary points in backside and frontside S_N2 reactions **1a**−**d** of $F^- + CH_3Y$, computed at ZORA-OLYP/TZ2P. [a] Nonexistent.

3. Results and Discussion

3.1. Reaction Profiles Backside S_N2-b. The results of our ZORA-OLYP/TZ2P calculations are collected in Table 1 (energies) and Figures 1−4 (geometries). The CH_3Y substrates, which are not contained in Figures 1−4, have C−Y bond distances of 1.396 Å (C−F), 1.791 Å (C−Cl), 1.959 Å (C−Br), and 2.157 Å (C−I). Full structural details can be found in Table S1 in the Supporting Information.

Most but not all of our model backside S_N2-b reactions (see Scheme 1) proceed via a double-well PES involving a central barrier and transition state (TS-b) as shown in Scheme 2a,b. We begin our exploration of reactivity with the trends along the backside S_N2-b substitutions in two series of reaction systems, **1b**−**4b**, in which the chloride nucleophile reacts with the four different halomethanes, and **2a**−**2d**, in which the four different halide nucleophiles react with chloromethane (see Scheme 1). Note that the two orthogonal series have the well-known $Cl^- + CH_3Cl$ reaction (2b) in common. The reactant and product complexes that are connected by the backside S_N2-b transition states in these two series are C_{3v} symmetric with a linear X−C−Y arrangement. They are stabilized with respect to the reactants and products, respectively by 6 to 19 kcal mol^{-1} (see Table 1).

As the nucleophile in $X^- + CH_3Cl$ is varied along $X^- = F^-$, Cl^-, Br^-, and I^-, the overall barrier (i.e., the energy of the TS-b relative to reactants R) increases monotonically from −19.2 to −0.2 to +4.1 to +7.9 kcal mol^{-1}, respectively (see Table 1, S_N2-b reactions 1b, 2b, 3b, 4b). Likewise, the central barrier (i.e., the energy of the TS-b relative to reactant complex RC-b) increases monotonically (from +0.2 to +8.8 to +11.4 to +14.1 kcal mol^{-1}, respectively), and the reaction energy changes from exothermic to increasingly endothermic (from −36.0 to 0.0 to +9.7 to +16.5 kcal mol^{-1}, respectively). Also the structural trends are nicely systematic with a TS-b for $X^- + CH_3Cl$ that becomes more and more product like along $X^- = F^-$, Cl^-, Br^-, and I^-, with an increasingly stretched carbon–leaving group (C−Cl) bond of 2.10, 2.36, 2.42, and 2.50 Å, respectively (see Figures 1−4).

On the other hand, variation of the leaving group in $Cl^- + CH_3Y$ along Y = F, Cl, Br, and I causes the overall barrier to monotonically *decrease* from +16.8 to −0.2 to −5.6 to −8.6 kcal mol^{-1} (see Table 1, S_N2-b reactions 2a, 2b, 2c, 2d), and again, the central barrier shows the same behavior: it decreases from +24.4 to +8.8 to +4.4 to +2.2 kcal mol^{-1}, respectively.

Similar trends occur along all other series of S_N2-b reaction systems: for a given leaving group, barriers increase as the nucleophile goes from fluoride to iodide; and for a given nucleophile, they decrease as the leaving group varies from fluorine to iodine. The two trends approximately cancel each other if both nucleophile and leaving group are symmetrically varied in $X^- + CH_3X$ along X = F, Cl, Br, and I: here, the overall barrier, for example, changes less, namely, from −7.6 to −0.2 to −1.7 to −1.9 kcal mol^{-1}, respectively (see Table 1, S_N2-b reactions 1a, 2b, 3c, 4d).

If the reaction exceeds a certain exothermicity (1c, 1d) or endothermicity (3a, 4a), the TS merges with the RC or PC, respectively (see Table 1). Consequently, the central barrier disappears for $F^- + CH_3Br$ or CH_3I (and the reverse S_N2-b reactions), and the reaction profile changes from double-well to single-well PES (see Scheme 2c).

3.2. Reaction Profiles Frontside S_N2-f. All of our frontside S_N2-f reactions are characterized by a double-well PES involving a central barrier and transition state (TS-f) as shown in Scheme 2a,b. They proceed from and to the same reactant (RC-b) and

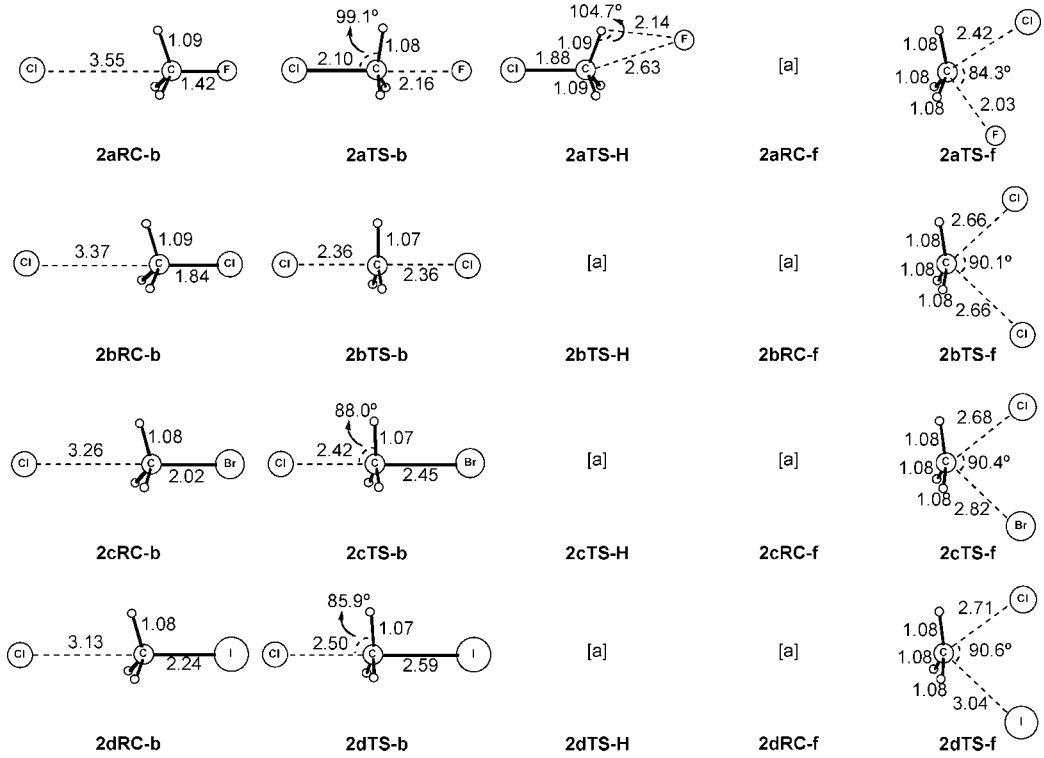

FIGURE 2. Structures (in angstroms, degrees) of stationary points in backside and frontside S_N2 reactions **2a**−**d** of $Cl^- + CH_3Y$, computed at ZORA-OLYP/TZ2P. [a] Nonexistent.

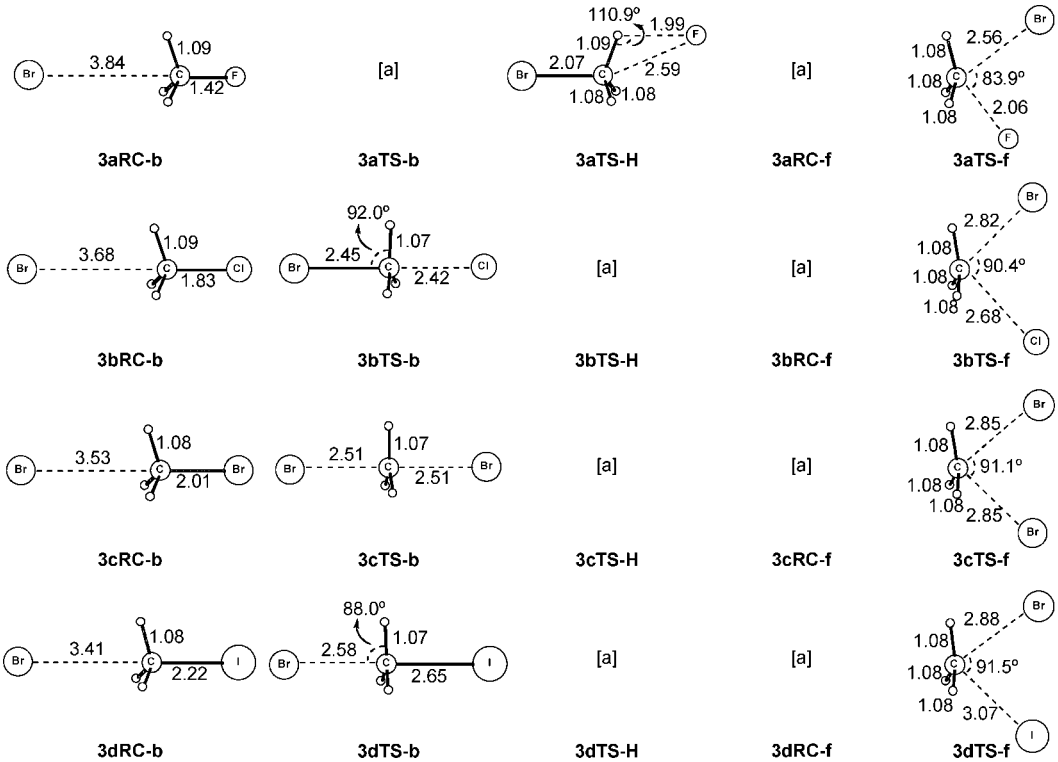

FIGURE 3. Structures (in angstroms, degrees) of stationary points in backside and frontside S_N2 reactions **3a**−**d** of $Br^- + CH_3Y$, computed at ZORA-OLYP/TZ2P. [a] Nonexistent.

product complexes (PC-b), respectively, as the backside S_N2-b reactions, unless such a complex involves a fluoride anion. In the latter case, the minimum energy path leads from the frontside transition state (TS-f) to separate frontside reactant (RC-f) or product complexes (PC-f) in which fluoride forms an F−H−C hydrogen bond with the methyl group of the neutral halomethane fragment (see Figures 1−4). Such a frontside complex has been reported also by Angel and Ervin[2] for the reaction of $F^- + CH_3Cl$.

The alternative "frontside complexes" RC-f and PC-f are about 2 kcal mol^{-1} more stable than the C_{3v} symmetric backside complexes RC-b and PC-b which are separated by slight barriers

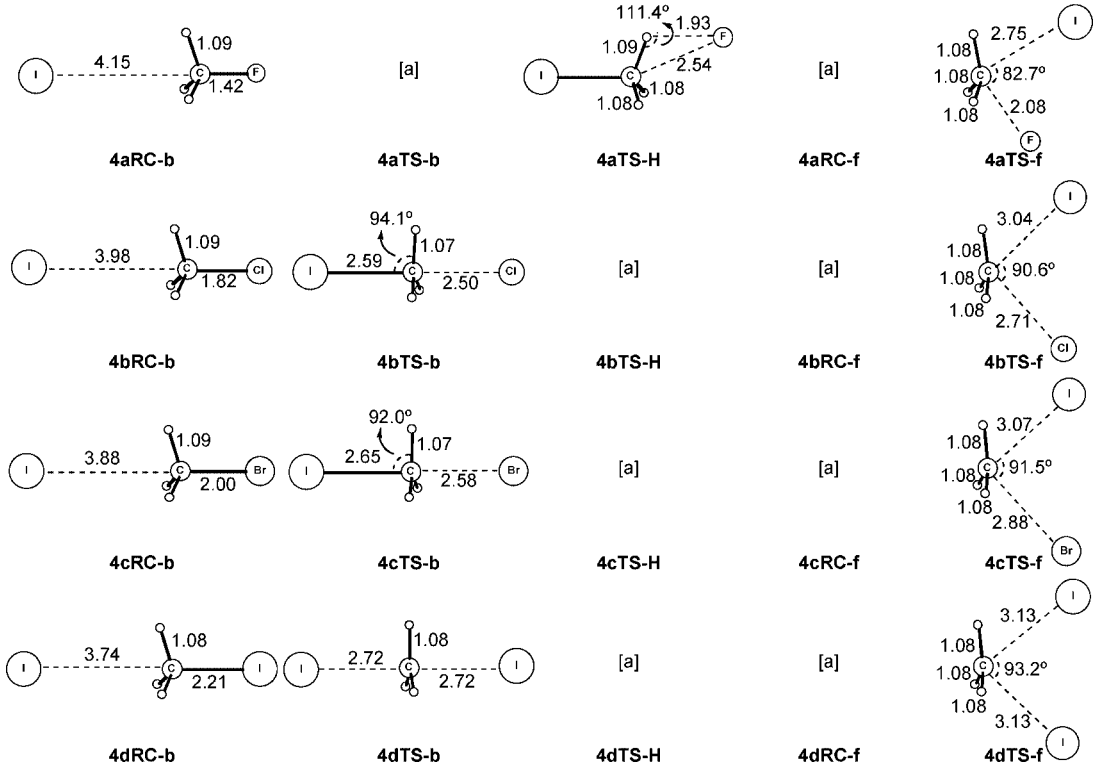

FIGURE 4. Structures (in angstroms, degrees) of stationary points in backside and frontside S_N2 reactions **4a**−**d** of $I^- + CH_3Y$, computed at ZORA-OLYP/TZ2P. [a] Nonexistent.

(TS-H) of only a few kcal mol^{-1} from the former (see Table 1). In the case of the single-well reactions of $F^- + CH_3Br$ or CH_3I (1c, 1d) and Br^- or $I^- + CH_3F$ (3a, 4a), in which the backside ion−molecule complexes are nonexistent as stable stationary points, the transition states TS-H separate the frontside complexes from the barrier-free backside substitution process.

The barriers of the frontside S_N2-f reactions are consistently higher by 36−41 kcal mol^{-1} than those of the backside S_N2-b reactions. Note, however, that the trends in reactivity for S_N2-f and S_N2-b are essentially equal. Thus, as the nucleophile in $X^- + CH_3Cl$ is varied along $X^- = F^-$, Cl^-, Br^-, and I^-, the overall frontside barrier (i.e., the energy of the TS-f relative to reactants R) increases monotonically from +19.4 to +40.2 to +43.3 to +45.4 kcal mol^{-1}, respectively (see Table 1, S_N2-f reactions 1b, 2b, 3b, 4b). Also the structural trends are nicely systematic with a TS-f for $X^- + CH_3Cl$ that becomes more and more product like along $X^- = F^-$, Cl^-, Br^-, and I^-, with an increasingly stretched carbon leaving group (C−Cl) bond of 2.42, 2.66, 2.68, and 2.71 Å, respectively (see Figures 1−4). Note that these C−Cl bonds in the various TS-f are consistently longer by 0.2−0.3 Å than those in the corresponding TS-b.

On the other hand, variation of the leaving group in $Cl^- + CH_3Y$ along Y = F, Cl, Br, and I causes the frontside overall barrier to monotonically *decrease* from +55.4 to +40.2 to +33.5 to +28.9 kcal mol^{-1} (see Table 1, S_N2-f reactions 2a, 2b, 2c, 2d).

Similar trends occur along all other series of S_N2-f reaction systems: for a given leaving group, barriers increase as the nucleophile goes from fluoride to iodide; and for a given nucleophile, they decrease as the leaving group varies from fluorine to iodine. Again, as in the case of the backside reactions, the two trends approximately cancel each other if both nucleophile and leaving group are symmetrically varied in $X^- + CH_3X$ along X = F, Cl, Br, and I: here, the frontside overall barrier, for example, changes less, namely, from +33.4 to +40.2 to +36.6 to +34.2 kcal mol^{-1}, respectively (see Table 1, S_N2-f reactions 1a, 2b, 3c, 4d).

3.3. Activation Strain Analyses: Nucleophilicity in S_N2-b. Next, we address the main purpose of our study: to understand *why*, for a given leaving group, the S_N2 barrier increases as the nucleophile goes from fluoride to iodide and *why*, for a given nucleophile, it decreases as the leaving group varies from fluorine to iodine. A model for arriving at such understanding emerges from our activation strain analyses[5,18] in which the potential energy surface $\Delta E(\zeta)$ of the model reactions is decomposed, along the reaction coordinate ζ, into the strain $\Delta E_{strain}(\zeta)$ associated with deforming the individual reactants plus the actual interaction $\Delta E_{int}(\zeta)$ between the deformed reactants (see section 2.2). The analysis results of the backside S_N2-b and frontside S_N2-f reactions are collected and visualized in Figures 5 and 6, respectively, which show potential energy surfaces $\Delta E(\zeta)$ (bold lines), strain energies $\Delta E_{strain}(\zeta)$ (plain lines), and interaction energies $\Delta E_{int}(\zeta)$ (dashed lines). Both figures are divided into a left and a right panel. The left panel addresses trends in nucleophilicity and contains four diagrams showing for each of the four leaving groups Y how the situation changes along the nucleophiles $X^- = F^-$, Cl^-, Br^-, and I^-. In an analogous manner, the right panel addresses trends in leaving-group ability and contains four diagrams showing for each of the four nucleophiles X^- how the situation changes along the leaving groups Y = F, Cl, Br, and I. The color code in each of the subdiagrams of Figures 5 and 6 is black, blue, red, and green as one goes along F, Cl, Br, and I.

A surprisingly clear picture emerges from the activation strain analyses. They show that nucleophilicity is determined in a straightforward manner by the electron-donor capability of the nucleophile (i.e., energy and shape of the X^- np atomic orbital), while leaving-group ability derives directly from the carbon–

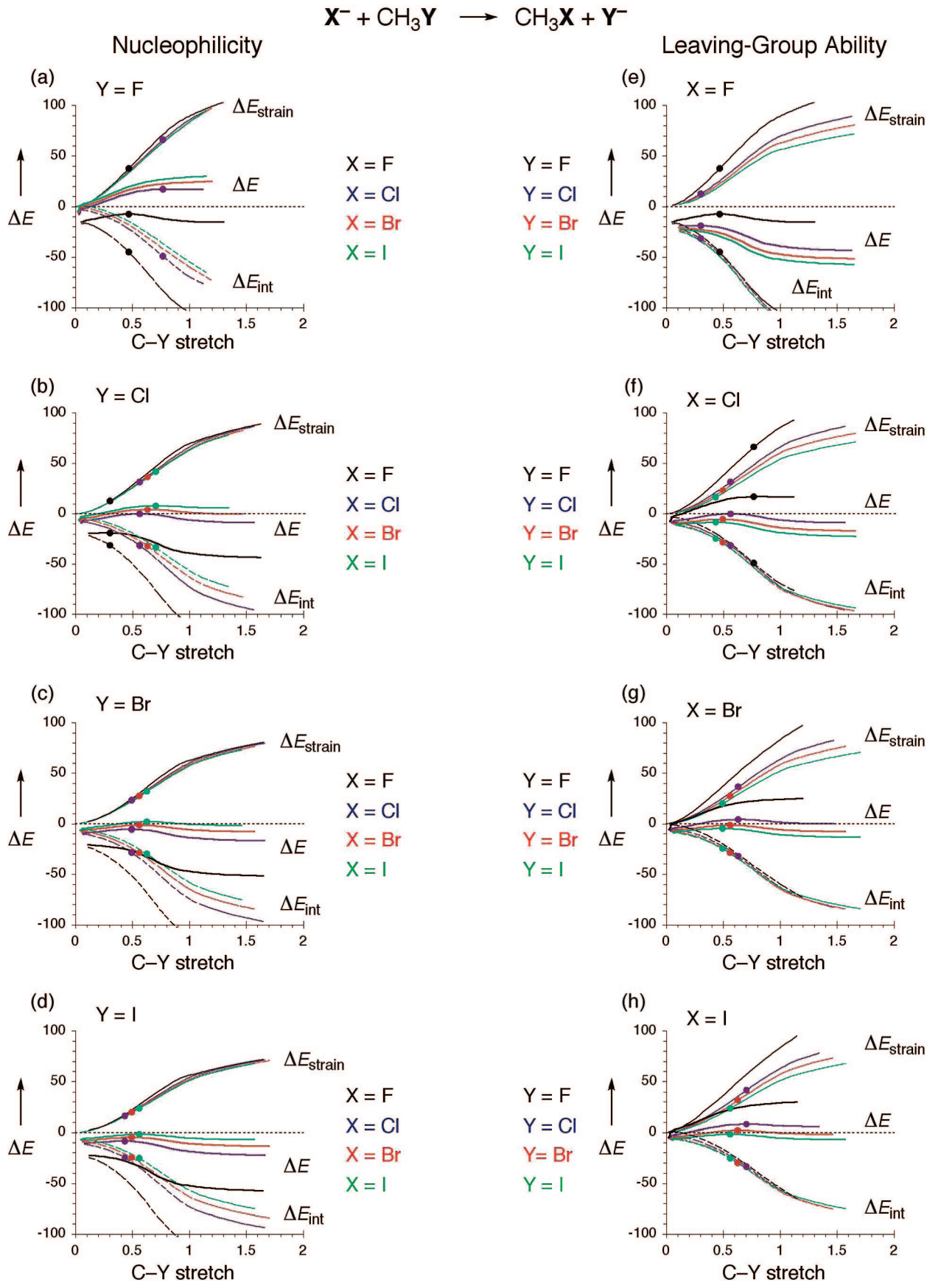

FIGURE 5. Activation strain analysis of backside S_N2 reaction profiles (in kcal mol^{-1}) along the reaction coordinate projected onto the C−Y stretch (in Å). Left panel: variation of nucleophile X^- for fixed leaving group Y. Right panel: variation of leaving group Y for fixed nucleophile X^-.

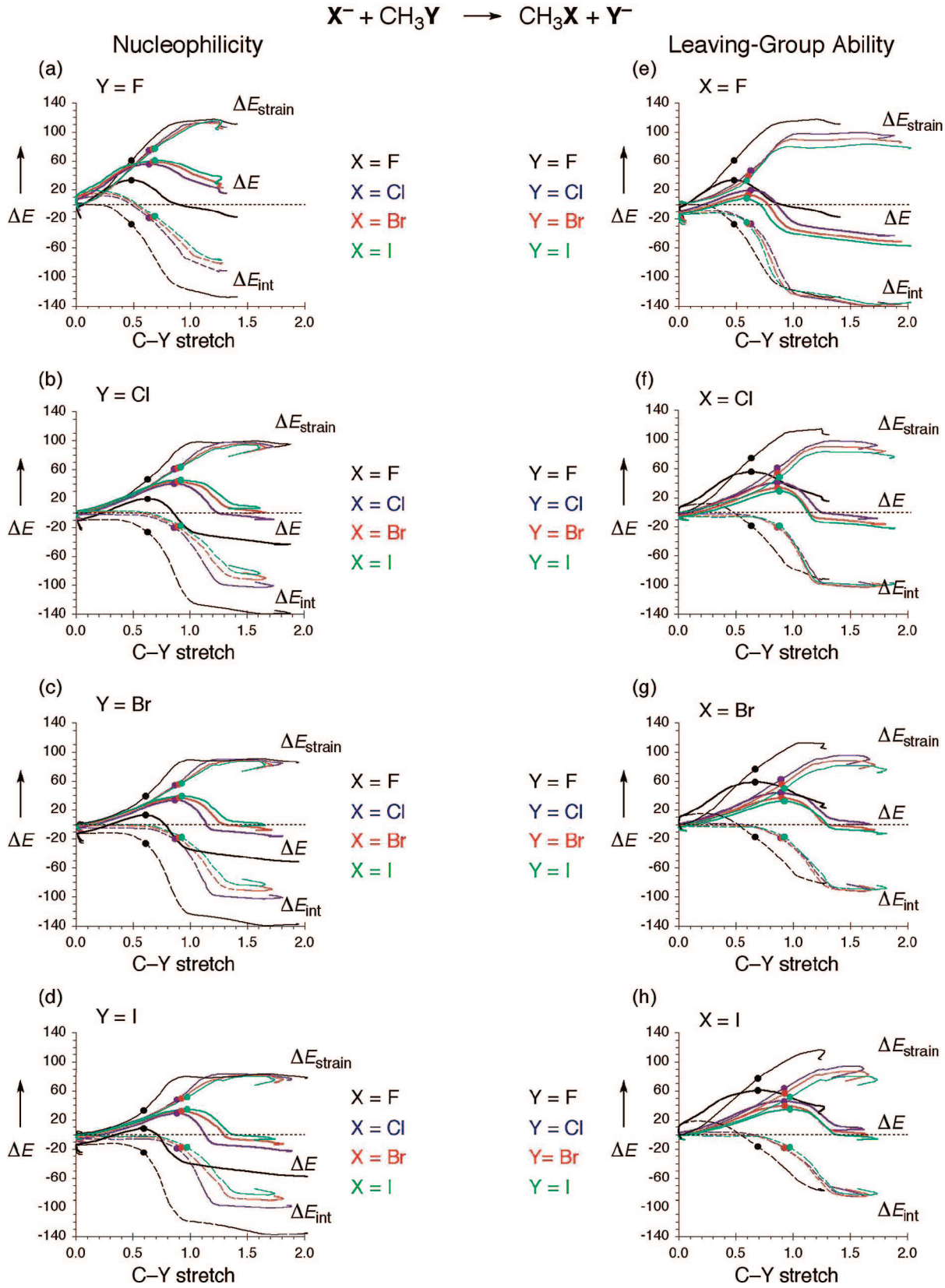

FIGURE 6. Activation strain analysis of frontside S_N2 reaction profiles (in kcal mol^{-1}) along the reaction coordinate projected onto the C−Y stretch (in Å). Left panel: variation of nucleophile X^- for fixed leaving group Y. Right panel: variation of leaving group Y for fixed nucleophile X^-.

leaving group (C−Y) bond strength. We first examine the trend in nucleophilicity along the four halide nucleophiles in backside S_N2-b reactions (Figure 5, left panel). We choose the reactions of $X^- + CH_3Cl$ for a detailed discussion but note that other leaving groups provide the same picture. Thus, as we go along $X^- = F^-$, Cl^-, Br^-, and I^-, we can see that the reaction profile

SCHEME 3. HOMO−LUMO Interaction of $X^- = F^-$, Cl^-, Br^-, and I^- with a Halomethane CH_3Y

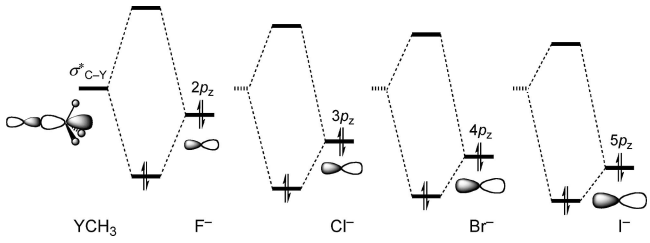

ΔE becomes more and more destabilized and the transition states (indicated by bullets) occur at still higher energies (see Figure 5b). Interestingly, this trend stems entirely from the interaction curves ΔE_{int} while the strain curves ΔE_{strain} of the four different reaction systems are nearly identical and superimposed (see Figure 5b). We come back to the strain curves ΔE_{strain} in section 3.4, where we discuss trends in leaving-group ability.

Note also that, if we go from $X^- = F^-$ to Cl^- to Br^- and to I^-, the transition states occur at still later points along the reaction coordinate (i.e., for larger C−Y stretch). This phenomenon, which is reminiscent of the Hammond postulate ("more endothermic reactions have more product-like transition states"), is the logical consequence of the fact that the transition state occurs at that point along the reaction coordinate ζ where $d\Delta E_{int}(\zeta)/d\zeta = -d\Delta E_{strain}(\zeta)/d\zeta$. Thus, as the $\Delta E_{int}(\zeta)$ curve becomes less stabilizing, its slope also diminishes, and the aforementioned condition is satisfied at a later, more product-like point along ζ.

We continue with the trend along interaction curves ΔE_{int} as they determine the trend along the nucleophiles. An analysis of the bonding mechanism behind this interaction curve shows that the dominant orbital interaction is the HOMO−LUMO interaction between the occupied X^- np AO pointing to the backside lobe of the empty CH_3Y σ^*_{C-Y} orbital. In all of the reactions, the interaction curve ΔE_{int} is stabilized as the reaction proceeds and the C−Y bond elongates. One reason is that the methyl group becomes more positively charged which leads to a better electrostatic attraction ΔV_{elstat}. The other important reason is that the C−Y antibonding σ^*_{C-Y} goes down in energy (smaller HOMO−LUMO gap) and gains more amplitude on the more electropositive methyl end of the substrate (better HOMO−LUMO overlap).

Importantly, regarding the trend in nucleophilicity, this HOMO−LUMO interaction becomes less stabilizing as the nucleophile is varied along $X^- = F^-$, Cl^-, Br^-, and I^-, which causes the observed destabilization in the ΔE_{int} curve and thus the overall reaction profile ΔE. The reason is that the orbital energy of the X^- np AO decreases in this order which causes the HOMO−LUMO gap to become larger and thus the orbital interaction ΔE_{oi} less stabilizing (see qualitative illustration in Scheme 3).

Note that this trend in orbital energies of the halide anions X^- runs counter to that in the neutral halogen atoms X. In the latter, the energy of the electronegative F 2p AO is lowest, and as the principal quantum number increases down the periodic table, the valence Cl 3p, Br 4p, and I 5p AOs become effectively more shielded and higher in energy. This is the orbital picture of the decreasing electronegativity along this series of halogens. However, if we put an excess electron on the halogens, the small and compact fluorine AOs experience more Coulomb repulsion and destabilization than in the case of the heavier and more diffuse halogens, which leads to the reversed trend in AO energies for the halide anions.

In conclusion, nucleophilicity is determined in a straightforward manner by the electron-donor capability of the nucleophile, that is, the energy (and shape; not discussed, here) of the X^- np atomic orbital. Thus, a higher X^- np orbital energy goes with a lower S_N2 barrier because of stronger, more stabilizing nucleophile−substrate interactions.

3.4. Activation Strain Analyses: Leaving-Group Ability in S_N2-b. Next, we examine the trend in leaving-group ability along the four halomethane substrates in backside S_N2-b reactions (Figure 5, right panel). We choose the reactions of $Cl^- + CH_3Y$ for a detailed discussion but note again that series with other nucleophiles provide the same picture. Thus, as we go along Y = F, Cl, Br, and I, we can see that the reaction profile ΔE becomes more and more *stabilized* and the transition states (indicated by bullets) occur at still lower energies along this series (see Figure 5f).

This time the trend stems entirely from the strain curves ΔE_{strain}, while now the interaction curves ΔE_{int} of the four different reaction systems are nearly identical and superimposed (see Figure 5f). The strain curves ΔE_{strain} become systematically destabilized as the leaving group varies along Y = F, Cl, Br, and I. A closer look at the origin of this behavior shows that it is directly related to the trend in the C−Y bond strengths: the H_3C-Y bond dissociation energy amounts to 113.7, 83.8, 71.3, and 60.0 kcal mol^{-1} along this series (see also ref 6). In fact, the strain curves ΔE_{strain} are very similar to the simple bond dissociation energy curves of the halomethanes involved. They differ, however, increasingly from the latter as the reaction approaches completion. This is because, in a simple dissociation, the halomethane transforms into a planar methyl radical plus a halogen atom, whereas along the S_N2-b reaction, the methyl moiety of the $[CH_3-Y]$ fragment adopts eventually again an (inverted) pyramidal configuration.

We conclude that leaving-group ability derives directly from carbon–leaving group (C−Y) bond strength. Thus, a stronger C−Y bond leads to a higher S_N2 barrier because of a higher, more *destabilizing* substrate strain.

3.5. Activation Strain Analyses: S_N2-f versus S_N2-b. The frontside S_N2-f barriers show, as pointed out above, the same trends as the backside ones: they increase along the nucleophiles F^-, Cl^-, Br^-, and I^- and decrease along the substrates CH_3F, CH_3Cl, CH_3Br, and CH_3I. They also have the same two origins (compare the corresponding diagrams in Figures 5 and 6). Thus, a higher X^- np orbital energy goes with a lower S_N2-f barrier because of stronger, more stabilizing nucleophile−substrate interactions ΔE_{int} (see Figure 6). On the other hand, a stronger C−Y bond leads to a higher S_N2-f barrier because of a higher, more *destabilizing* substrate strain ΔE_{strain} (see again Figure 6).

The higher frontside S_N2-f as compared to backside S_N2-b barriers have been previously attributed to less efficient <nucleophile HOMO | substrate LUMO> overlap and thus less stabilizing nucleophile−substrate interaction ΔE_{int}[22] (see Scheme 4). Previously, we have shown this mechanism to be partially responsible for the higher S_N2-f than S_N2-b barrier for $Cl^- + CH_3Cl$,[8] and here, we find that indeed also for all other combinations of $X^- + CH_3Y$, the interaction curves ΔE_{int} are less stabilizing in the early parts of the reaction process (up until the transition states) of the frontside substitutions (compare corresponding reaction systems in Figures 5 and 6). This

(22) Anh, N. T.; Minot, C. *J. Am. Chem. Soc.* **1980**, *102*, 103.

SCHEME 4. Overlap between X^- np HOMO and CH_3Y σ^*_{C-Y} LUMO in S_N2-b and S_N2-f

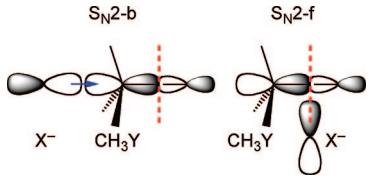

constitutes a significant contribution to the higher energy of the frontside as compared to the backside reaction profiles ΔE.

Interestingly, however, the main reason for the higher barrier for frontside substitution is the increased steric repulsion between nucleophile X and leaving group Y, which are adjacent in the TS for frontside S_N2-f while they are on opposite sides of the trigonal bipyramidal transition structure for backside S_N2-b. The proximity of the two large X and Y groups in the frontside TS-f translates into a more deformed substrate in the frontside S_N2-f processes and thus to the higher-energy strain curves ΔE_{strain} (compare Figures 5 and 6). This constitutes the main source of the higher-energy frontside reaction profiles ΔE. Note that this is also the reason for the above-mentioned larger C−X and C−Y distances in the frontside transition states TS-f as compared to the backside transition states TS-b (see Figures 1−4).

4. Conclusions

In conclusion, our analyses of the backside and frontside S_N2 reactions of $X^- + CH_3Y$ (X, Y = halogen), based on relativistic density functional theory, yield a consistent overview of trends and a clear picture of what makes a good or poor nucleophile or leaving group. In line with previous experimental and theoretical work, we find that backside S_N2-b barriers increase along the nucleophiles F^-, Cl^-, Br^-, and I^- and decrease along the substrates CH_3F, CH_3Cl, CH_3Br, and CH_3I. Frontside S_N2-f barriers show the same trends but are in all cases much higher (ca. 10−60 kcal mol^{-1}) because of more steric repulsion as a result of the proximity between the nucleophile and leaving group.

Our analyses of these trends, based on the activation strain model of chemical reactivity (see Theoretical Methods for details), yield a clear picture of what makes a good nucleophile or leaving group in the sense of yielding a low S_N2 barrier. Nucleophilicity is determined in a straightforward manner by the electron-donor capability of the nucleophile (i.e., energy and shape of the X^- np atomic orbital), whereas leaving-group ability derives directly from carbon–leaving group (C−Y) bond strength.

Thus, a higher X^- np orbital energy goes with a lower S_N2 barrier (both backside and frontside) because of stronger, more stabilizing nucleophile−substrate interactions. On the other hand, a stronger C−Y bond leads to a higher S_N2 barrier (both backside and frontside) because of a higher, more *destabilizing* substrate strain. An interesting next step is to explore how the introduction of a solvent interferes with these basic principles. This will contribute to a more complete picture of the factors that determine relative rates of condensed-phase S_N2 reactions.

Acknowledgment. We thank The Netherlands Organization for Scientific Research (NWO-CW) for financial support.

Supporting Information Available: Cartesian coordinates of all species occurring in our model reactions and complete ref 10. This material is available free of charge via the Internet at http://pubs.acs.org.

JO801215Z